crystals

MDPI

Article

Structural Insights into the Two-Step Spin-Crossover Compound Fe(3,4-dimethyl-pyridine)$_2$[Ag(CN)$_2$]$_2$

José Alberto Rodríguez-Velamazán [1,*], Kosuke Kitase [2], Elías Palacios [3], Miguel Castro [3], Ángel Fernández-Blanco [1], Ramón Burriel [3] and Takafumi Kitazawa [2]

1 Institut Laue-Langevin, 71 Avenue des Martyrs, CS 20156-38042 Grenoble, France; fernandez-blanco@ill.eu
2 Department of Chemistry, Faculty of Science, Toho University, Miyama, Funabashi, Chiba 274-8510, Japan; 6117004k@st.toho-u.ac.jp (K.K.); kitazawa@chem.sci.toho-u.ac.jp (T.K.)
3 Instituto de Ciencia de Materiales de Aragón (ICMA), CSIC—Universidad de Zaragoza, 50009 Zaragoza, Spain; elias@unizar.es (E.P.); mcastro@unizar.es (M.C.); burriel@unizar.es (R.B.)
* Correspondence: velamazan@ill.eu; Tel.: +33-(0)47-620-7260

Received: 24 May 2019; Accepted: 16 June 2019; Published: 19 June 2019

Abstract: The crystal structure of the polymeric spin crossover compound Fe(3,4-dimethyl-pyridine)$_2$[Ag(CN)$_2$]$_2$ has been solved and its temperature dependence followed by means of single-crystal and powder X-ray diffraction. This compound presents a two-step spin transition with relatively abrupt steps centred at ca. 170 K and 145 K and a plateau at around 155 K. The origin of the two-step transition is discussed in light of these structural studies. The observations are compatible with a mostly disordered state between the two steps, consisting of mixing of high-spin and low-spin species, while weak substructure reflections in the mixed phase could indicate some degree of long-range order of the high-spin and low-spin sites.

Keywords: iron (II), spin crossover; X-ray diffraction; coordination polymers

1. Introduction

The quest for switchable magnetic compounds represents one of the major topics in the field of molecular magnetism. One of the most typical examples of molecular switching in the solid state is that of spin-crossover (SCO) compounds. These systems can interconvert between low-spin (LS) and high-spin (HS) states as a result of different stimuli, like a change in temperature, pressure, the application of electric and magnetic fields, by light irradiation, or by adsorption/desorption of guest molecules [1–5].

It is well-known that the SCO phenomenon is explained from ligand-field theory considerations [6]. The LS state is the ground-state of SCO compounds, being the stable state at low temperatures and involving high ligand-field strength, while the HS state becomes stable at high temperatures and involves low ligand-field strength [7]. Usually, the LS to HS spin transition encompasses an increase of the metal–ligand bond lengths and, indeed, the interplay between the ligand field strength dependence on the metal–ligand distance and the electron–electron repulsion can be considered the mainspring for the SCO [6]. Most commonly, spin crossover compounds contain Fe(II) in a $3d^6$ electronic configuration, the spin transition occurring between a diamagnetic LS state (S = 0) and a paramagnetic HS state (S = 2), and a number of them present an N_6 first coordination sphere. For these compounds, the change in the Fe–N distances from the LS to the HS state is typically ~0.2 Å [8,9]. The structure around the central ions has therefore a particular relevance for understanding the properties of these compounds [10].

A particularly successful synthetic route for spin-crossover compounds with interesting functional properties is that of the SCO Hofmann-type coordination polymers, where cyanometalate complexes connect the SCO centres forming extended networks with different dimensionalities

and topologies [11,12]. Since the first compound of this type reported by Prof. Kitazawa in 1996 [13], a number of SCO compounds with a large display of functional properties have been described [3,14]. Some time ago we reported the synthesis and characterisation of the 2D spin-crossover compound $Fe(py)_2[Ag(CN)_2]_2$ (py = pyridine) [15], and later we described the magnetic, photomagnetic, calorimetric, Mössbauer and reflectivity studies of the derived $Fe(X\text{-}py)_2[Ag(CN)_2)]_2$ family (X = H; 3-methyl; 4-methyl; 3,4-dimethyl; 3-Cl) [16]. The main characteristic of this series is the two-step character of the transitions in most of the compounds, which is also observed in the relaxation of the photoinduced HS metastable state. The compounds derived by halogen substitution in the position 3 of the pyridine, $Fe(3\text{-}Xpy)_2[M(CN)_2]_2$ (X = F, Cl, Br, I and M = Ag, Au) have been reported by the group of Prof. J. A. Real [17,18]. The 3-Fpy derivatives also present two-step transitions (at ambient pressure for the Ag compound and at 0.18–0.26 GPa for the Au one). In turn, the use of the bicyclic ligand 1,6-naphthyridine, has allowed a wide thermal hysteresis centred near room temperature to be obtained [19]. In other closely related systems, also derived from $[M^I(CN)_2]^-$ (M^I = Ag, Au) building blocks, like $Fe(3\text{-F-}4\text{-methyl-py})_2[Au(CN)_2]_2$ [20] or $Fe(4\text{-}(3\text{-pentyl})py)_2[Au(CN)_2]_2$ [21], two-step transitions are also observed. Finally, opening the focus to the Fe(II) Hofmann-like coordination polymers constituted of $[M^{II}(CN)_4]^{2-}$ (MII = Ni, Pd, Pt) building blocks, multistep spin transitions are also found [22,23]. Therefore, it is worth trying to shed light on the origin of this frequent feature in this type of compounds. In some of the cited cases, a structural inequivalence of different SCO sites in the intermediate phases is at the origin of the multistep behaviour [22]. But, unfortunately, there is a lack of precise structural information of some of these systems due to the difficulties in obtaining single crystals. In this work we report on the structure of $Fe(3,4\text{-dimethyl-pyridine})_2[Ag(CN)_2]_2$. This compound shows a clear two-step behaviour in the magnetic susceptibility and heat capacity curves in the region of the spin transition [16], which starts at ca. 200 K and spans in a temperature range of around 90 K with a plateau at around 155 K (Figure 1a). The relatively abrupt steps are centred at ca. 170 K and 145 K, with around 47% and 53% of spin conversion, respectively, and with practical absence of residual fraction of high-spin species at low temperature [16]. In this work, the crystal structure of $Fe(3,4\text{-dimethyl-pyridine})_2[Ag(CN)_2]_2$ has been solved and its temperature dependence followed by means of single-crystal and powder X-ray diffraction.

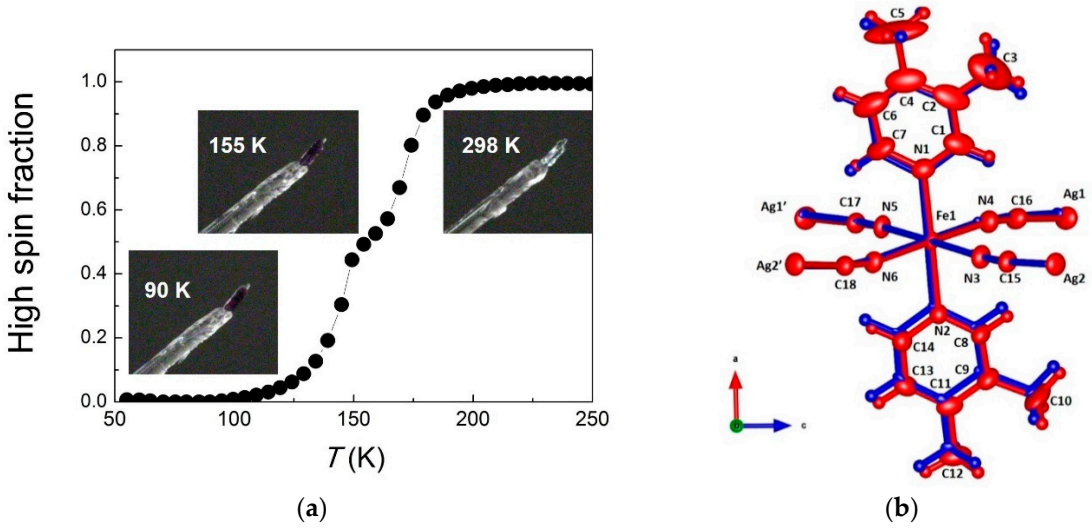

Figure 1. (**a**) Temperature dependence of the fraction of centres in the high-spin state for $Fe(3,4\text{-dimethyl-pyridine})_2[Ag(CN)_2]_2$ deduced from magnetic susceptibility measurements (from Reference [16]) and photographs of the crystals at the temperatures of the structural determination. (**b**) Representation of a fragment of the structure of $Fe(3,4\text{-dimethyl-pyridine})_2[Ag(CN)_2]_2$ at room temperature (red) and 90 K (blue) containing its asymmetric unit and atom numbering (excepting H atoms, for clarity). Thermal ellipsoids of non-hydrogen atoms are represented at 40% probability (H atoms are represented as spheres with arbitrary radius).

2. Materials and Methods

Fe(3,4-dimethyl-pyridine)$_2$[Ag(CN)$_2$]$_2$ was synthesized as described previously [15,16]. Single crystals were formed by a slow diffusion method after more than 2 days at room temperature from an aqueous mixture of (i) $FeSO_4(NH_4)_2SO_4{\cdot}6H_2O$ and 3,4-dimethyl-pyridine in 10 mL of water and (ii) K[Ag(CN)$_2$] in 10 mL of water. The colour of the samples changed from white (powder)/colourless (crystals) at room temperature (HS) to purple at low temperature (LS). The elemental analysis of the samples confirmed the organic contents.

The crystal structures were determined by single-crystal X-ray diffraction using a BRUKER APEX SMART CCD (Bruker, Billerica, MA, USA) area-detection diffractometer with monochromatized Mo *Kα* radiation (λ = 0.71 Å) at 298 K, 155 K and 90 K. The diffraction data were treated using SMART and SAINT (Bruker (2012). Bruker AXS Inc., Madison, WI, USA), while the absorption corrections were performed using SADABS [24]. The structures were solved by direct methods with SHELXTL [25]. All non-hydrogen atoms were refined anisotropically, and the hydrogen atoms were generated geometrically. Graphical representations of the structures were produced using the program VESTA [26]. COD 3000244 and 3000245 contain the Supplementary Materials crystallographic data for this paper. These data can be obtained free of charge via http://www.crystallography.net/search.html.

Powder X-ray diffraction patterns were recorded at room temperature, 210 K, 155 K and 80 K using a D-max Rigaku system, with a Cu rotating anode generator operated at 35 kV, 80 mA and a graphite monochromator to select the CuKα radiation. Step-scanned patterns were measured between 2Θ = 5° and 60° (in steps of 0.03°). Data have been analysed using the FULLPROF program [27].

3. Results and Discussion

The crystal structure of Fe(3,4-dimethyl-pyridine)$_2$[Ag(CN)$_2$]$_2$ in both the HS and LS states was determined by single-crystal X-ray diffraction at room temperature and 90 K, respectively. At these temperatures the crystals of this compound are respectively colourless and purple (Figure 1a), which is an indication of the spin transition. An additional structural determination was performed in the plateau region, at 155 K (see below). The compound crystallizes in the monoclinic $P2_1/c$ space group, which is maintained after the spin transition. There is only one crystallographically independent Fe(II) site in both high-temperature and low-temperature structures. The Fe(II) atom is surrounded by six N atoms corresponding to four CN groups belonging to two crystallographically independent $[Ag(CN)_2]^-$ units in the equatorial positions and two 3,4-dimethyl-pyridine ligands in the axial ones (Figure 1b).

At room temperature, we distinguish two types of Fe–N bond distances, the axial ones [Fe–N(1) = 2.211(4) Å; Fe–N(2) = 2.208(4) Å] being longer than the equatorial ones [Fe–N(3) = 2.155(4) Å; Fe–N(4) = 2.162(4) Å; Fe–N(5) = 2.162(4) Å; Fe–N(6) = 2.180(4) Å] (Figure 1). These Fe–N distances were consistent with a HS state. The two independent $[Ag(CN)_2]^-$ units were very similar and display an almost linear geometry; the C–Ag–C bond angle is in the 175.7(6)–177.9(2)° range. These groups connect two iron atoms defining chains parallel to the diagonals of the *bc*-plane, thus forming two-dimensional corrugated layers (Figure 2). The layers are organized in pairs, held together by strong argentophilic interactions (Figure 2), which are attractive interactions occurring between silver centres when two or more low-coordinated silver cations appear in pairs or groups in molecular structures with distances between them lower than the sum of van der Waals radii of Ag atoms (3.44 Å) [28]. The Ag–Ag distance in the double layer is 2.9853(7) Å, while the distance between double layers is 7.1273(8) Å. The two-dimensional mesh is penetrated by the 3,4-dimethyl-pyridine ligands from the upper and lower layers. The stacking of the pyridine rings was held by π−π interactions. Some of the displacement ellipsoids of C atoms, in particular those of the methyl groups, are significantly larger than in the rest of the structure (Figure 1), probably a consequence of some degree of disorder (static or dynamic) in these groups involving uncertainty in the position of H atoms.

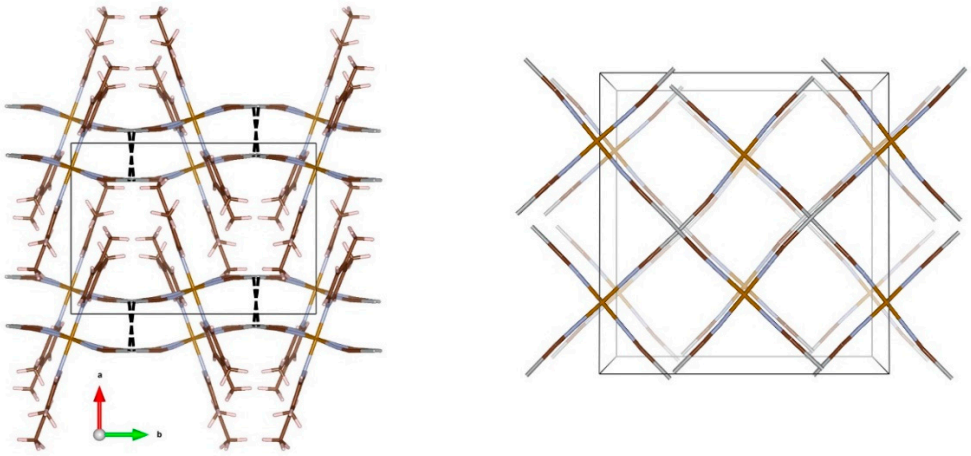

(**a**) (**b**)

Figure 2. View of the relative disposition of the layers of Fe(3,4-dimethyl-pyridine)$_2$[Ag(CN)$_2$]$_2$. (**a**) Stacking of four consecutive layers along the [001] direction. The dashed lines show the argentophilic interactions. (**b**) View of the relative disposition of two grids along the [100] direction. Colour code: iron: yellow; silver: grey; nitrogen: light blue; carbon: brown; hydrogen: light pink.

At 90 K, the structure is isostructural with that at room temperature, but with significant changes related with the spin transition. An overall contraction of the cell is observed (Table 1), and is more relevant in the *bc*-plane (parallel to the 2D layers) than in the *a*-direction. The most significant changes are those associated with the contraction produced in the [FeN$_6$] coordination octahedron associated with the spin transition. The average Fe–N bond distance shortens by 0.219 Å, as expected for a complete SCO in an iron(II) complex. Again we distinguish two types of Fe–N bond distances, the axial ones [Fe–N(1) = 1.997(5) Å; Fe–N(2) = 2.001(4) Å], longer than the equatorial ones [Fe–N(3) = 1.939(4) Å; Fe–N(4) = 1.943(4) Å; Fe–N(5) = 1.942(4) Å; Fe–N(6) = 1.940(3) Å] (Figure 1). The contraction in the *bc*-plane results in slightly more corrugated 2D layers. The Ag–Ag distance in the double layer is reduced to 2.9263(6) Å, while the distance between double layers is slightly increased to 7.1300(11) Å as a consequence of the transition. The larger displacement ellipsoids observed at high temperature are no more present at low temperature; however, the methyl groups make a slight turn to accommodate in the LS structure (Figure 1).

Table 1. Crystallographic data for Fe(3,4-dimethyl-pyridine)$_2$[Ag(CN)$_2$]$_2$ at different temperatures.

Formula	**C$_{18}$ H$_{18}$ Ag$_2$ Fe N$_6$**		
Formula weight		589.97	
T (K)	298 K	155 K	90 K
Crystal system	monoclinic	monoclinic	monoclinic
Space Group	*P* 2$_1$/*c*	*P* 2$_1$/*c*	*P* 2$_1$/*c*
Z	4	4	4
a (Å)	10.0093(8)	9.898(8)	9.9550(13)
b (Å)	15.0039(11)	14.609(12)	14.2900(19)
c (Å)	14.8435(11)	14.573(12)	14.3979(19)
β (°)	91.4390(10)	91.356(10)	91.090(2)
V (Å^3)	2228.5(3)	2107(3)	2047.8(5)
Fe–N(1) (Å)	2.211(4)	2.09(2)	1.997(5)
Fe–N(2) (Å)	2.208(4)	2.08(2)	2.001(4)
Fe–N(3) (Å)	2.155(4)	2.01(2)	1.939(4)
Fe–N(4) (Å)	2.162(4)	2.08(3)	1.943(4)
Fe–N(5) (Å)	2.162(4)	2.03(3)	1.942(4)
Fe–N(6) (Å)	2.180(4)	2.04(3)	1.940(3)
No. of measured, independent and observed [$I > 2\sigma(I)$] reflections (R_{int})	10391, 3404, 2672 (0.023)	9951, 3900, 2788 (0.084)	13965, 4884, 4043 (0.030)
$R[F^2 > 2\sigma(F^2)]$, $wR(F^2)$, *S*	0.030, 0.067, 1.04	0.109, 0.313, 1.85	0.040, 0.141, 1.01

The evolution with temperature of the crystal structure of Fe(3,4-dimethyl-pyridine)$_2$[Ag(CN)$_2$]$_2$ across the spin transition was followed by powder X-ray diffraction. The pattern at room temperature perfectly agrees with the structure determined by single-crystal diffraction (Figure 3) without any modification of the structural parameters. On lowering the temperature, the pattern at 210 K (just above the transition) closely resembles the diffractogram at room temperature. Changes in some intensities are observed at 155 K (in the plateau of the spin transition), in particular in the 25° < 2Θ < 30° region, with the pattern appearing as a mixture of those at room temperature and 80 K, where the diffractogram again corresponds with the structure determined by single-crystal diffraction in the LS state at 90 K. The cell volume decreases continuously with temperature, with the contraction being more pronounced in the region of the spin transition. The volume decrease is mainly due to the contraction in the *bc*-plane, with the *b* and *c* axes showing little variation between room temperature and 210 K, and decreasing significantly with the spin transition (ca. 4%). The *a*-axis shows the opposite behaviour, with a relatively smaller overall contraction (ca. 0.6 % in the whole temperature range) and only a slight variation in the region of the spin transition; in particular, an anomalous increase is observed in the *a*-axis in the low temperature step of the transition (the axial Fe–N bonds are approximately in this direction). The evolution of the lattice parameters can be observed by following the position of the reflections (0 2 2)—*bc*-plane—and (2 0 0) —*a*-axis—in the diffraction patterns shown in the inset of Figure 3-left, while the lattice parameters and cell volume obtained from the fit of the diffractograms are shown in Figure 3-middle and right, respectively.

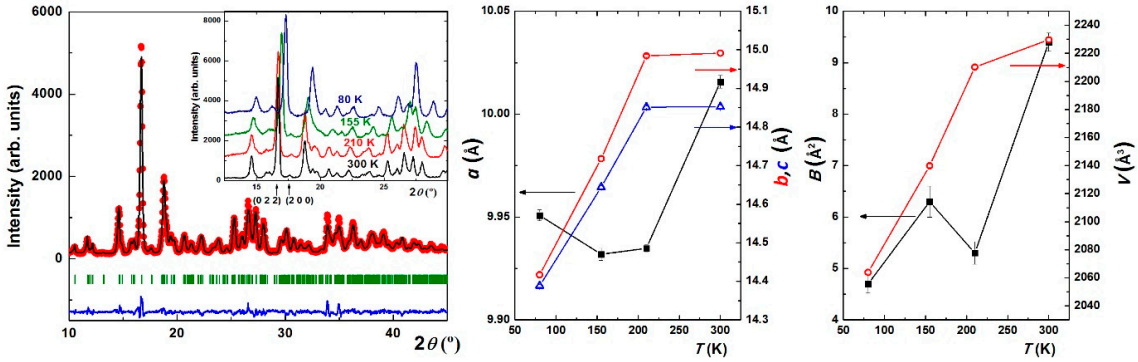

Figure 3. Left: Powder X-ray diffraction pattern of Fe(3,4-dimethyl-pyridine)$_2$[Ag(CN)$_2$]$_2$ at room temperature. Experimental (red symbols) and calculated patterns (black line), and Bragg peak positions (vertical green marks). Inset: detail of the experimental patterns at room temperature, 210 K, 155 K and 80 K; the arrows indicate the positions of the (0 2 2) and (2 0 0) reflections. **Middle**: lattice parameters obtained by powder X-ray diffraction vs. temperature. **Right**: thermal displacement parameter and cell volume vs. temperature.

From the magnetic measurements, we can infer that the proportion of iron centres in the HS and LS states in the plateau region is around one-half/one-half (see Figure 1a and Reference [16]). Nothing in the powder diffraction patterns suggests that these are distributed in an ordered way, which, together with the fact that a single crystallographically independent Fe site is present in both the HS and LS structures, rather supports a scenario with an equal mixture of HS and LS species not ordered at long range, in the same way as in the Fe(pyridine)$_2$[Ag(CN)$_2$]$_2$ compound [15]. In line with this scenario, if we refine an overall "thermal" displacement factor, *B*, as a function of temperature (together with the cell parameters, but keeping invariant the rest of the structural parameters determined by single-crystal diffraction), we observe an anomalous increase in the region of the plateau of the spin transition (Figure 3-right), which is consistent with having an average of Fe(II) ions in two different spin states. The spin transition involves a significant change in the Fe–N distance, and therefore the anomalous "thermal" factor is in this case due to positional disorder caused by the presence of HS and LS species in the same crystallographic position.

The single-crystal data at 155 K can be interpreted as well as a structure described in the monoclinic $P2_1/c$ space group, with only one crystallographically independent Fe(II) site. However, the quality of the refinement is poorer as a result of the disorder related with the coexistence of HS and LS states and the presence of twinning. In particular, some atomic displacement ellipsoids present an abnormal shape, due to the uncertainty in the distances, specifically those that are more affected by the change in spin state. In agreement with the powder diffraction results, the *a*-axis appears anomalously more contracted than at 90 K, although the cell volume follows a continuous decrease with temperature. In the single-crystal data, there are some weak but observed reflections at 155 K of type (h0l) with l = odd, i.e., forbidden by the $P2_1/c$ space group (unobserved in the powder diffraction data). These reflections would indicate two non-equivalent Fe sites, and some degree of order in the position of the atoms in HS and LS state, although crystal twinning could account (at least in part) for these forbidden reflections. A refinement with the triclinic space group *P*-1 was also tested. The refined cell has alpha = 90.11(2)°, beta = 91.53(1)°, gamma = 91.22(2)°. The results in the *P*-1 group show very slightly shorter Fe–N distances in one of the two inequivalent Fe sites, being in all cases intermediate between those at room temperature and at 90 K. This can be interpreted as though, most probably, a symmetry breaking occurs in the plateau region implying some order of HS and LS species, but cannot be clearly resolved due to a low degree of long-range ordering (disorder) and twinning. Refining the data in the *P*-1 group gives very similar results as for the $P2_1/c$ group, and the use of the less symmetric group is therefore not clearly justified. Then, the most plausible situation is a distribution of HS and LS species with a low degree of long-range order (and probably with some short-range order, but the present diffraction experiments are not sensitive to it). This kind of mostly disordered state has been explained for previously reported examples [15,29] as a result of competing long and short-range ferro- and antiferro-elastic interactions, respectively, between SCO centres, transmitted via the bonds of the polymeric network.

4. Conclusions

We have investigated the origin of the two-step spin-crossover transition of Fe(3,4-dimethyl-pyridine)$_2$[Ag(CN)$_2$]$_2$ by means of single-crystal and powder X-ray diffraction. The structure has been solved in both high-spin (room temperature) and low-spin states (90 K). The structure is described in the monoclinic $P2_1/c$ space group, which is maintained across the spin transition, with a single crystallographically independent Fe(II) site. The observations in the plateau region between the two steps of the spin transition (155 K) are compatible with a state between the two steps consisting of an equal mixture of high-spin and low-spin species with a low degree of long-range order.

Supplementary Materials: Supplementary crystallographic data at 155 K are available online at http://www.mdpi.com/2073-4352/9/6/316/s1.

Author Contributions: Conceptualization, J.A.R.-V.; Data curation, K.K., Á.F.-B. and T.K.; Formal analysis, K.K. and E.P.; Funding acquisition, M.C. and R.B.; Investigation, J.A.R.-V., K.K., E.P. and T.K.; Supervision, J.A.R.-V., M.C., R.B. and T.K.; Visualization, Á.F.-B.; Writing—original draft, J.A.R.-V.; Writing—review & editing, E.P., M.C., Á.F.-B. and R.B.

Funding: This research was funded by the Spanish Ministerio de Ciencia, Innovación y Universidades (grant numbers MAT2015-68200-C02-2-P and MAT2017-86019-R) and Diputación General de Aragón (Project E11-17R).

Acknowledgments: The authors acknowledge the use of Servicios Generales de Apoyo a la Investigación from Universidad de Zaragoza and thank Takayuki Suda in Department of Chemistry, Toho University for his contribution in the preparation of the compound.

Conflicts of Interest: The authors declare no conflict of interest. The funders had no role in the design of the study; in the collection, analyses, or interpretation of data; in the writing of the manuscript, or in the decision to publish the results.

References

1. Linert, W.; Verdaguer, M. *Molecular Magnets: Recent Highlights*; Springer: Wien, Austria, 2003.
2. Gutlich, P.; Goodwin, H.A. Topics in Current Chemistry. In *Spin-Crossover in Transition Metal Compounds*; Springer: Berlin, Germany, 2004.
3. Muñoz, M.C.; Real, J.A. Thermo-, piezo-, photo- and chemoswitchable spin crossover iron(II) metallocyanate based coordination polymers. *Coord. Chem. Rev.* **2011**, *255*, 2068–2093. [CrossRef]
4. Halcrow, M.A. *Spin-Crossover Materials: Properties and Applications*; John Wiley & Sons: Chichester, UK, 2013.
5. Senthil Kumar, K.; Ruben, M. Emerging trends in spin crossover (SCO) based functional materials and devices. *Coord. Chem. Rev.* **2017**, *346*, 176–205. [CrossRef]
6. Hauser, A. Ligand Field Theoretical Considerations. *Top. Curr. Chem.* **2004**, *233*, 49–58.
7. Gütlich, P.; Goodwin, H. Spin Crossover—An Overall Perspective. *Top. Curr. Chem.* **2004**, *233*, 1–47.
8. König, E. Nature and dynamics of the spin-state interconversion in metal complexes. *Struct. Bond.* **1991**, *76*, 51–152.
9. Collet, E.; Guionneau, P. Structural analysis of spin-crossover materials: From molecules to materials. *C. R. Chim.* **2018**, *21*, 1133–1151. [CrossRef]
10. Guionneau, P.; Marchivie, M.; Bravic, G.; Létard, J.-F.; Chasseau, D. Structural Aspects of Spin Crossover. Example of the $[Fe^{II}Ln(NCS)_2]$ Complexes. *Top. Curr. Chem.* **2004**, *234*, 97–128.
11. Garcia, Y.; Niel, V.; Muñoz, M.C.; Real, J.A. Spin crossover in 1D, 2D and 3D polymeric Fe(II) networks. *Top. Curr. Chem.* **2004**, *233*, 229–257.
12. Sciortino, N.F.; Neville, S.M. Two-Dimensional Coordination Polymers with Spin Crossover Functionality. *Aust. J. Chem.* **2014**, *67*, 1553–1562. [CrossRef]
13. Kitazawa, T.; Gomi, Y.; Takahasi, M.; Takeda, M.; Enomoto, M.; Miyazaki, A.; Enoki, T. Spin-crossover behaviour of the coordination polymer $Fe^{II}(C_5H_5N)_2Ni^{II}(CN)_4$. *J. Mater. Chem.* **1996**, *6*, 119–121. [CrossRef]
14. Ni, Z.-P.; Liu, J.-L.; Hogue, N.; Liu, W.; Li, J.-Y.; Chen, Y.-C.; Tong, M.-L. Recent advances in guest effects on spin-crossover behavior in Hofmann-type metal-organic frameworks. *Coord. Chem. Rev.* **2017**, *335*, 28–43. [CrossRef]
15. Rodríguez-Velamazán, J.A.; Castro, M.; Palacios, E.; Burriel, R.; Kitazawa, T.; Kawasaki, T. A Two-Step Spin Transition with a Disordered Intermediate State in a New Two-Dimensional Coordination Polymer. *J. Phys. Chem. B* **2007**, *111*, 1256–1261. [CrossRef] [PubMed]
16. Rodríguez-Velamazán, J.A.; Carbonera, C.; Castro, M.; Palacios, E.; Kitazawa, T.; Létard, J.F.; Burriel, R. Two-Step Thermal Spin Transition and LIESST Relaxation of the Polymeric Spin-Crossover Compounds $Fe(X\text{-}py)_2[Ag(CN)_2]_2$ (X=H, 3-methyl, 4-methyl, 3,4-dimethyl, 3-Cl). *Chem. Eur. J.* **2010**, *16*, 8785–8796. [CrossRef] [PubMed]
17. Muñoz, M.C.; Gaspar, A.B.; Galet, A.; Real, J.A. Spin-Crossover Behavior in Cyanide-Bridged Iron(II)-Silver(I) Bimetallic 2D Hofmann-like Metal-Organic Frameworks. *Inorg. Chem.* **2007**, *46*, 8182–8192. [CrossRef] [PubMed]
18. Agustí, C.; Muñoz, M.C.; Gaspar, A.B.; Real, J.A. Spin-Crossover Behavior in Cyanide-bridged Iron(II)-Gold(I) Bimetallic 2D Hofmann-like Metal-Organic Frameworks. *Inorg. Chem.* **2008**, *47*, 2552–2561. [CrossRef] [PubMed]
19. Hiiuk, V.M.; Shova, S.; Rotaru, A.; Ksenofontov, V.; Fritsky, I.O.; Gural'skiy, I.A. Room temperature hysteretic spin crossover in a new cyanoheterometallic framework. *Chem. Commun.* **2019**, *55*, 3359–3362. [CrossRef] [PubMed]
20. Kosone, T.; Kawasaki, T.; Tomori, I.; Okabayashi, J.; Kitazawa, T. Modification of Cooperativity and Critical Temperatures on a Hofmann-Like Template Structure by Modular Substituent. *Inorganics* **2017**, *5*, 55. [CrossRef]
21. Kosone, T.; Kitazawa, T. Guest-dependent spin transition with long range intermediate state for 2-dimensional Hofmann-like coordination polymer. *Inorg. Chim. Acta* **2016**, *439*, 159–163. [CrossRef]
22. Sciortino, N.F.; Scherl-Gruenwald, K.R.; Chastanet, G.; Halder, G.J.; Chapman, K.W.; Letard, J.-F.; Kepert, C.J. Hysteretic Three-Step Spin Crossover in a Thermo- and Photochromic 3D Pillared Hofmann-type Metal-Organic Framework. *Angew. Chem. Int. Ed.* **2012**, *51*, 10154–10158. [CrossRef]

23. Kucheriv, O.I.; Shylin, S.I.; Ksenofontov, V.; Dechert, S.; Haukka, M.; Fritsky, I.O.; Gural'skiy, I.A. Spin Crossover in Fe(II)–M(II) Cyanoheterobimetallic Frameworks (M = Ni, Pd, Pt) with 2-Substituted Pyrazines. *Inorg. Chem.* **2016**, *55*, 4906–4914. [CrossRef]
24. Sheldrick, G.M. *SADABS Program for Empirical Absorption Correction for Area Detector Data*; University of Göttingen: Göttingen, Germany, 1996.
25. Sheldrick, G.M. *SHELXTL Program for the Solution of Crystal Structure*; University of Göttingen: Göttingen, Germany, 1997.
26. Momma, K.; Izumi, F. VESTA 3 for three-dimensional visualization of crystal, volumetric and morphology data *J. Appl. Crystallogr.* **2011**, *44*, 1272–1276. [CrossRef]
27. Rodríguez-Carvajal, J. Recent advances in magnetic structure determination by neutron powder diffraction. *Phys. B* **1993**, *192*, 55–69. [CrossRef]
28. Schmidbaur, H.; Schier, A. Argentophilic Interactions. *Angew. Chem. Int. Ed.* **2015**, *54*, 746–784. [CrossRef] [PubMed]
29. Romstedt, H.; Hauser, A.; Spiering, H.; Gutlich, P. Modelling of two step high spin⇌ low spin transitions using the cluster variation method. *J. Phys. Chem. Solids* **1998**, *59*, 1353–1362. [CrossRef]